Mitochondrial dysfunction due to long-chain Acyl-CoA dehydrogenase deficiency causes hepatic steatosis and hepatic insulin resistance

Dongyan Zhang*, Zhen-Xiang Liu*, Cheol Soo Choi†, Liqun Tian‡, Richard Kibbey†, Jianying Dong*, Gary W. Cline†, Philip A. Wood‡, and Gerald I. Shulman*†§¶

*Howard Hughes Medical Institute and Departments of †Internal Medicine and §Cellular and Molecular Physiology, Yale University School of Medicine, New Haven, CT 06510; and ‡Department of Genetics, University of Alabama at Birmingham, Birmingham, AL 35294

Contributed by Gerald I. Shulman, August 1, 2007 (sent for review July 7, 2006)

Alterations in mitochondrial function have been implicated in the pathogenesis of insulin resistance and type 2 diabetes. However, it is unclear whether the reduced mitochondrial function is a primary or acquired defect in this process. To determine whether primary defects in mitochondrial β-oxidation can cause insulin resistance, we studied mice with a deficiency of long-chain acyl-CoA dehydrogenase (LCAD), a key enzyme in mitochondrial fatty acid oxidation. Here, we show that LCAD knockout mice develop hepatic steatosis, which is associated with hepatic insulin resistance, as reflected by reduced insulin suppression of hepatic glucose production during a hyperinsulinemic-euglycemic clamp. The defects in insulin action were associated with an ≈40% reduction in insulin-stimulated insulin receptor substrate-2-associated phosphatidylinositol 3-kinase activity and an ≈50% decrease in Akt2 activation. These changes were associated with increased PKCε activity and an aberrant 4-fold increase in diacylglycerol content after insulin stimulation. The increase in diacylglycerol concentration was found to be caused by *de novo* synthesis of diacylglycerol from medium-chain acyl-CoA after insulin stimulation. These data demonstrate that primary defects in mitochondrial fatty acid oxidation capacity can lead to diacylglycerol accumulation, PKCε activation, and hepatic insulin resistance.

diacylglycerol | mitochondria | nonalcoholic fatty liver disease | PKCε

Recent studies have implicated alterations in mitochondrial function in the pathogenesis of insulin resistance and type 2 diabetes mellitus (1–8). It has been proposed that decreased mitochondrial fatty acid oxidation can result in insulin resistance by promoting increased intracellular diacylglycerol content, which in turn leads to activation of novel PKCs in liver and skeletal muscle and decreased insulin signaling and action in these tissues (9). However, it remains to be determined whether reduced mitochondrial function plays a primary role in causing the insulin resistance or whether it is a result of the increase in intracellular lipid content or other acquired factors (6, 10). To address this question, we examined insulin action in liver and skeletal muscle, using the hyperinsulinemic-euglycemic clamp, in long-chain acyl-CoA dehydrogenase (LCAD)-deficient ($LCAD^{-/-}$) mice, a genetic model of defective fatty acid oxidation. LCAD is a mitochondrial matrix enzyme catalyzing the first step for the oxidation of long-chain fatty acyl-CoAs. $LCAD^{-/-}$ mice are known to have impaired fatty acid oxidation and develop a disease similar to other disorders of mitochondrial fatty acid oxidation (11–12). We also examined the impact of LCAD deficiency on whole-body glucose and fatty acid oxidation in these mice, using indirect calorimetry.

Results

Metabolic Profile of the $LCAD^{-/-}$ Mice. $LCAD^{-/-}$ mice, fed a standard rodent diet, had similar body weights but a 60% increase in whole-body fat content compared with their WT littermates (Table 1). However, they ate 11% less of the standard rodent diet compared with the WT littermates. Basal plasma concentrations of glucose, insulin, fatty acids, β-hydroxybutyrate, and triglyceride were similar in the two groups. Interestingly, plasma cholesterol levels were 2-fold higher in the $LCAD^{-/-}$ mice compared with the WT control mice. There were no differences in plasma concentrations of adiponectin, IL-6, TNFα, or resistin between the two groups of mice. Consistent with the increase in fat mass leptin concentrations were 80% higher in the $LCAD^{-/-}$ mice compared with the WT controls.

Hepatic Insulin Resistance and Reduced Insulin Signaling in Livers of $LCAD^{-/-}$ Mice. The metabolic consequences of impaired fatty acid oxidation were examined during a 2-h hyperinsulinemic-euglycemic clamp in awake 12-week-old WT control and $LCAD^{-/-}$ mice. No significant differences were observed in the glucose infusion rate (Fig. 1*A*) required to maintain euglycemia during the clamp or in insulin-stimulated whole-body glucose metabolism (Fig. 1*B*). Consistent with these data, no differences were found in insulin-stimulated 2-deoxyglucose uptake in skeletal muscle (Fig. 1*D*) during the clamp between the two groups. In contrast, insulin-stimulated suppression of hepatic glucose production during the clamp was markedly lower in the $LCAD^{-/-}$ mice compared with the WT mice (Fig. 1*C*; $LCAD^{-/-}$, 24% vs. control, 67% suppression; $P < 0.01$), indicating severe hepatic insulin resistance in the $LCAD^{-/-}$ mice.

Consistent with the decrease in insulin suppression of hepatic glucose production observed during the clamp, insulin-stimulated insulin receptor substrate (IRS)-2 tyrosine phosphorylation in the liver of the $LCAD^{-/-}$ mice was reduced by 50% in the $LCAD^{-/-}$ mice compared with the WT littermates (Fig. 1*E*). Furthermore, insulin-stimulated IRS-2-associated phosphatidylinositol (PI)3-kinase activity and Akt2 activity were also decreased by 35% and 50%, respectively (Fig. 1 *F* and *G*), in the livers of the $LCAD^{-/-}$ mice compared with WT controls. No differences were found in IRS-1-associated PI3-kinase activity in skeletal muscle of the $LCAD^{-/-}$ mice compared with the WT littermates (Fig. 1*H*).

Insulin Stimulation Leads to Increases in Diacylglycerol Content and PKCε Activity in Liver. After an overnight fast, intracellular diacylglycerol and ceramide content in liver were similar between the two

Author contributions: D.Z., Z.-X.L., C.S.C., G.W.C., P.A.W., and G.I.S. designed research; D.Z., Z.-X.L., C.S.C., L.T., R.K., J.D., G.W.C., and P.A.W. performed research; P.A.W. contributed new reagents/analytic tools; D.Z., Z.-X.L., C.S.C., L.T., R.K., J.D., G.W.C., P.A.W., and G.I.S. analyzed data; and D.Z., Z.-X.L., C.S.C., L.T., R.K., J.D., G.W.C., P.A.W., and G.I.S. wrote the paper.

The authors declare no conflict of interest.

Freely available online through the PNAS open access option.

Abbreviations: LCAD, long-chain acyl-CoA dehydrogenase; IRS, insulin receptor substrate; PI, phosphatidylinositol.

¶To whom correspondence should be addressed. E-mail: gerald.shulman@yale.edu.

This article contains supporting information online at www.pnas.org/cgi/content/full/0707060104/DC1.

MEDICAL SCIENCES

Table 1. Metabolic profile in plasma of the WT and *LCAD*$^{-/-}$ mice

Parameter	*n*	WT	*LCAD*$^{-/-}$
Body weight, g	9	26.4 ± 0.8	28.0 ± 0.9
Lean body mass, g	9	19.8 ± 0.5	20.0 ± 0.6
Whole-body fat content, % body weight	9	8.1 ± 0.5	13.1 ± 1.2*
Food intake, kcal·kg^{-1}·d^{-1}	16	611 ± 22	547 ± 15*
Glucose, mg/dl	9	176 ± 7.3	154 ± 26
Insulin, pM	9	98 ± 12	103 ± 11
Adiponectin, μg/ml	10	5.9 ± 0.7	5.8 ± 0.9
Leptin, ng/ml	10	5.7 ± 1.3	10.1 ± 1.7*
Resistin, ng/ml	10	5.9 ± 1.9	4.3 ± 0.6
IL-6, pg/ml	10	49 ± 27	15 ± 5.3
TNFα, pg/ml	10	6.2 ± 0.8	6.4 ± 0.7
Fatty acid, mM	6	0.52 ± 0.13	0.63 ± 0.08
Triglyceride, mM	6	49 ± 4.4	62 ± 6
β-Hydroxybutyrate, mM	6	0.26 ± 0.06	0.20 ± 0.03
Total cholesterol, mg/dl	6	73 ± 6.3	142 ± 5.9*

Whole-body fat content was obtained from awake mice with a Bruker Mini-Spec analyzer. Data are presented as mean ± SEM. *, $P < 0.05$ compared with WT controls.

groups of mice (Fig. 2*A*). However, insulin stimulation led to a 4-fold increase in diacylglycerol content in the *LCAD*$^{-/-}$ mice compared with the fasting state, with no change observed in the insulin-sensitive WT mice (Fig. 2*B*). In contrast, there were no changes in liver ceramide content after insulin stimulation in either group.

Studies have suggested a strong link between hepatic insulin resistance and PKCε activation (13). Because PKCε is activated by diacylglycerol through membrane translocation, we measured the PKCε membrane translocation in these mice. Consistent with the lack of differences in intrahepatic diacylglycerol content in the basal state, there were no differences in PKCε membrane translocation in the liver of the *LCAD*$^{-/-}$ mice compared with WT controls under fasting conditions (Fig. 2*C*). However, after insulin stimulation and a 4-fold increase in intrahepatic diacylglycerol content, PKCε membrane to cytosolic ratio increased >2-fold in the *LCAD*$^{-/-}$ mice compared with WT littermates (Fig. 2*D*).

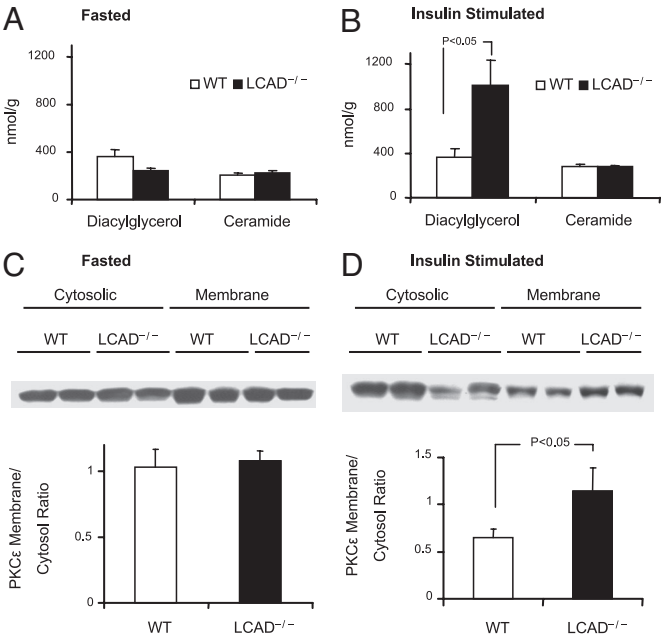

Fig. 2. Hepatic insulin resistance in *LCAD*$^{-/-}$ mice is associated with increased insulin-stimulated diacylglycerol content and PKCε membrane translocation. (*A*) Liver diacylglycerol content at basal fasting condition. (*B*) Liver diacylglycerol content after the hyperinsulinemic-euglycemic clamp. (*C*) Western blot analysis of basal liver cytosolic and membranal PKCε. (*D*) Western blot analysis of cytosolic and membranal PKCε in livers of mice after clamp.

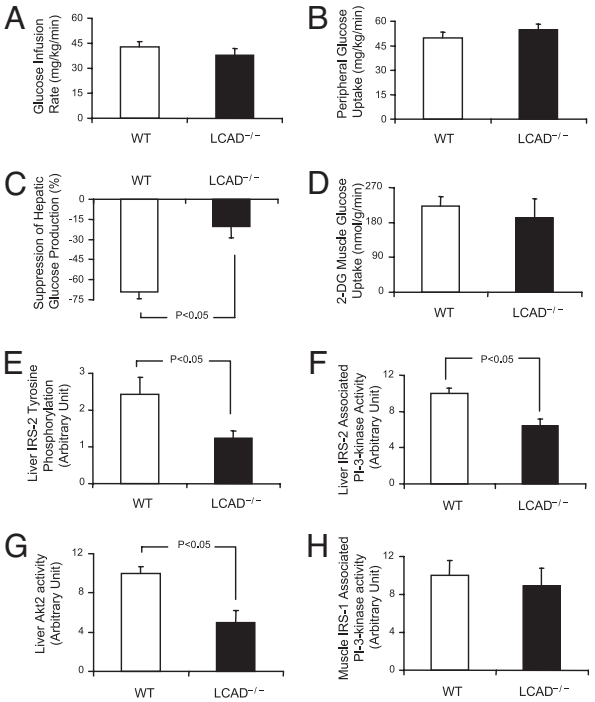

Fig. 1. Whole-body glucose metabolism and insulin signaling in WT (open bars) and *LCAD*$^{-/-}$ (filled bars) mice during the hyperinsulinemic-euglycemic clamp. (*A*) Glucose infusion rate averaged for the last 30 min of the clamp. (*B*) Whole-body glucose disposal rate during the clamp. (C) Suppression of hepatic glucose production during the clamp. (*D*) Rate of insulin-stimulated muscle glucose uptake. (*E*) Liver IRS2 tyrosine phosphorylation. (*F*) Liver PI3-kinase activity. (*G*) Liver Akt2 activity. (*H*) Muscle IRS-1-associated PI3-kinase activity.

Insulin-Stimulated Increases in Hepatic Diacylglycerol Content Can Be Attributed to Increased *de Novo* Synthesis. Increases in intrahepatocellular diacylglycerol have been implicated in fat-induced insulin resistance, but whether the diacylglycerol comes from membrane lipid lipolysis or from *de novo* synthesis is not clear. *LCAD*$^{-/-}$ mice provide an excellent model to examine the potential contribution of *de novo* synthesis to the cellular diacylglycerol pool because these mice accumulate medium-chain acyl-CoAs, especially $C_{14:1}$ acyl-CoA (Fig. 3*A*), as a result of their inability to oxidize these metabolites. In *LCAD*$^{-/-}$ mice, insulin stimulation caused an increase in hepatic diacylglycerol content (Fig. 3*B*) and a decrease of the medium-chain acyl-CoAs content (Fig. 3*C*). Fig. 4 is a schematic diagram showing oleic acid metabolism in the fasting (Fig. 4 *A* and *B*) and fed (Fig. 4 *C* and *D*) WT and *LCAD*$^{-/-}$ mice, respectively. To investigate whether acyl-CoA conversion to diacylglycerol was a major contributing factor for the accumulation of diacylglycerol in the *LCAD*$^{-/-}$ mice, we infused uniformly labeled [^{13}C]oleic acid during a hyperinsulinemic-euglycemic clamp. The liver profiles of acyl-CoA and diacylglycerol were subsequently analyzed to obtain the percentage enrichment of the species of interest (Table 2). Because incorporation of the $C_{14:1}$ group directly into diacylglycerol was minimal (D.Z. and G.I.S., unpublished data), we measured incorporation of both [$^{13}C_{18}$]oleoyl-CoA and [$^{13}C_{14}$]tetradecenoyl-CoA into diacylglycerol in the form of oleoyl groups. The diacylglycerols we measured were diolein, oleoyl linolein, and oleoyl palmitoin, because they accounted for a majority of the increase of diacylglycerols after insulin stimulation (Fig.

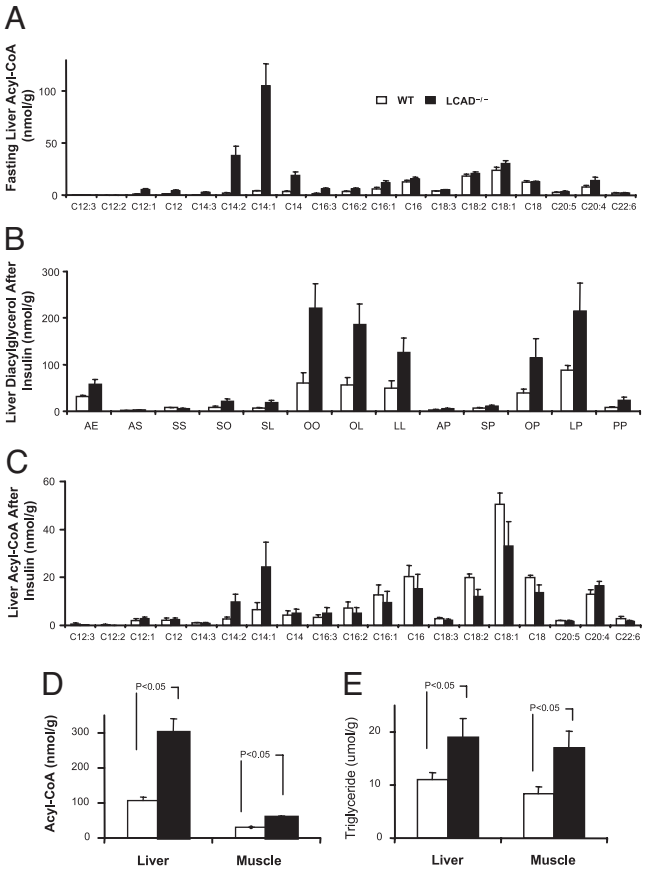

Fig. 3. Profile and contents of acyl-CoA, diacylglycerol and triglyceride in liver and muscle. (*A*) Liver fasting acyl-CoA profile. (*B*) Liver diacylglycerol profile after insulin clamp. A, E, S, O, L, and P denote arachidonoyl, eicosapentanoyl, stearoyl, oleoyl, linoleoyl, and palmitoyl groups, respectively. (*C*) Acyl-CoA profile after insulin clamp. (*D*) Acyl-CoA content. (*E*) Triglyceride content.

3*C*). Enrichment of the [$^{13}C_{18}$]oleoyl group in these diacylglycerols (M + 18) was similar in WT and *LCAD*$^{-/-}$ mice (Table 2). However, enrichment of the [$^{13}C_{14}$]tetradecenoyl group into these diacylglycerols (M + 14) as a percentage of enrichment in $C_{14:1}$-CoA was 5- to 7-fold higher in *LCAD*$^{-/-}$ mice compared with WT controls (Table 2). These data suggest that there is a very active pathway of chain elongation of $C_{14:1}$-CoA into oleoyl-CoA and subsequent esterification into diacylglycerol in the *LCAD*$^{-/-}$ mice, and the activity of this pathway during insulin stimulation led to the accumulation of diacylglycerols.

Energy Homeostasis and Regulation of Fatty Acid Oxidation and Triglyceride Synthesis. We also analyzed energy homeostasis in these mice, using indirect calorimetry. The percentage of fatty acid and glucose oxidation was derived from the respiratory quotient, assuming that contributions from other sources of energy substrates, such as amino acids, were minimal. Compared with the WT control mice, *LCAD*$^{-/-}$ mice lacked diurnal variation and had a 27% decrease (calculated from area under the curves of Fig. 5*A*, $P < 0.01$) in the overall percentage of fatty acid oxidation during the day time, when the mice were not eating (Fig. 5*A*). Interestingly, despite the absence of a key enzyme in mitochondrial β-oxidation, the *LCAD*$^{-/-}$ mice had a 29% increase in the percentage of fatty acid oxidation ($P < 0.01$) compared with WT controls during the dark period, when they were eating (Fig. 5*A*). Overall, the percentage of fatty acid oxidation was 11% lower in *LCAD*$^{-/-}$ mice compared with WT control mice. Interestingly physical activity (Fig. 5*B*), at the onset of the dark phase, increased >90% in the *LCAD*$^{-/-}$ mice compared with WT control mice ($P < 0.05$, calculated from the area under the curve). Overall oxygen consumption (Fig. 5*C*) and energy expenditure (Fig. 5*D*) were 7% lower ($P < 0.05$) in the *LCAD*$^{-/-}$ mice. However, because overall food intake (Fig. 5*E*) was also lower in the *LCAD*$^{-/-}$ mice (15%, $P < 0.05$), net daily energy balance as calculated from energy intake minus energy expenditure was not different in the two groups (WT, 92 ± 19 kcal/kg/d vs. *LCAD*$^{-/-}$, 72 ± 16 kcal·kg^{-1}·d^{-1}, $P = 0.4$).

Quantitative RT-PCR was used to measure liver expression of genes involved in fatty acid oxidation (Table 3). Gene expression of the microsomal fatty acid ω-hydroxylase, CYP4A1, increased 5-fold, and expression of peroxisomal acyl-CoA oxidase mRNA increased 2-fold, whereas the mitochondrial CPT2 increased 30%. However, expression of VLCAD, MCAD, CPT1a, and PPARα were not altered. In addition, no differences were found in mitochondrial DNA content in either liver or muscle between *LCAD*$^{-/-}$ mice and WT control mice (data not shown).

Total intracellular acyl-CoA content increased 180% and 90% in liver and skeletal muscle, respectively, in the *LCAD*$^{-/-}$ mice compared with the WT control mice (Fig. 3*D*). Tissue triglyceride content increased 70% and 100% in liver and skeletal muscle, respectively, in the *LCAD*$^{-/-}$ mice compared with the control mice (Fig. 3*E*). To see whether these changes were caused by gene expression, we measured RNA expression of the major genes involved in hepatic triglyceride metabolism and found no differences in SREBP1c, ChREBP, ACC1, SCD1, DAGT2, hormone-sensitive lipase (HSL), and adipocyte triacylglycerol lipase (ATGL) mRNAs (Table 3) except for an increase in expression of PPARγ and triglyceride hydrolase (TGH). Because there was an increase in plasma cholesterol content in the LCAD$^{-/-}$ mice, we measured gene expression of SREBP2, LXRα, and HMG-CoA reductase (HMGR), but no difference was found.

Discussion

Here, we show that a primary defect in mitochondrial fatty acid oxidation in the *LCAD*$^{-/-}$ mice leads to increased triglyceride storage in both muscle and liver and severe hepatic insulin resistance, which was associated with a defect in insulin signal transduction at the level of IRS-2 tyrosine phosphorylation. Moreover, we show that protein kinase Cε is activated after insulin stimulation, which coincided with an increase in hepatocellular diacylglycerol content, suggesting that an aberrant increase in hepatic diacylglycerol synthesis after insulin stimulation was most likely responsible for the hepatic insulin resistance in these mice.

Adipocytokines have also been implicated in causing hepatic insulin resistance (14–16). However, hepatic insulin resistance in *LCAD*$^{-/-}$ mice could not be attributed to changes in circulating adiponectin, IL-6, TNFα, or resistin concentrations, because the plasma levels of these adipocytokines in the *LCAD*$^{-/-}$ mice were not different from the plasma levels in the WT mice. Although plasma leptin concentrations were higher in the *LCAD*$^{-/-}$ mice, a higher leptin concentration would be expected to have the opposite effects on insulin sensitivity and was most likely secondary to the increase in fat mass in the *LCAD*$^{-/-}$ mice.

Through the action of protein kinase Cε, diacylglycerol has been implicated as the causative metabolite in fat-induced hepatic insulin resistance by directly binding to and inhibiting insulin receptor tyrosine kinase activity (17). Interestingly, although diacylglycerol content was not elevated under basal conditions, hepatic diacylglycerol content increased 4-fold after insulin stimulation in the *LCAD*$^{-/-}$ mice. Protein kinase Cε activity was also found to be increased under these conditions. These data support the hypothesis that diacylglycerol activation of protein kinase Cε plays a major role in causing hepatic insulin resistance in the *LCAD*$^{-/-}$ mice. However, in contrast to a recent study implicating ceramide as the causative factor in mediating fat-induced insulin resistance (18), we did not find any changes in ceramide content in liver of these mice,

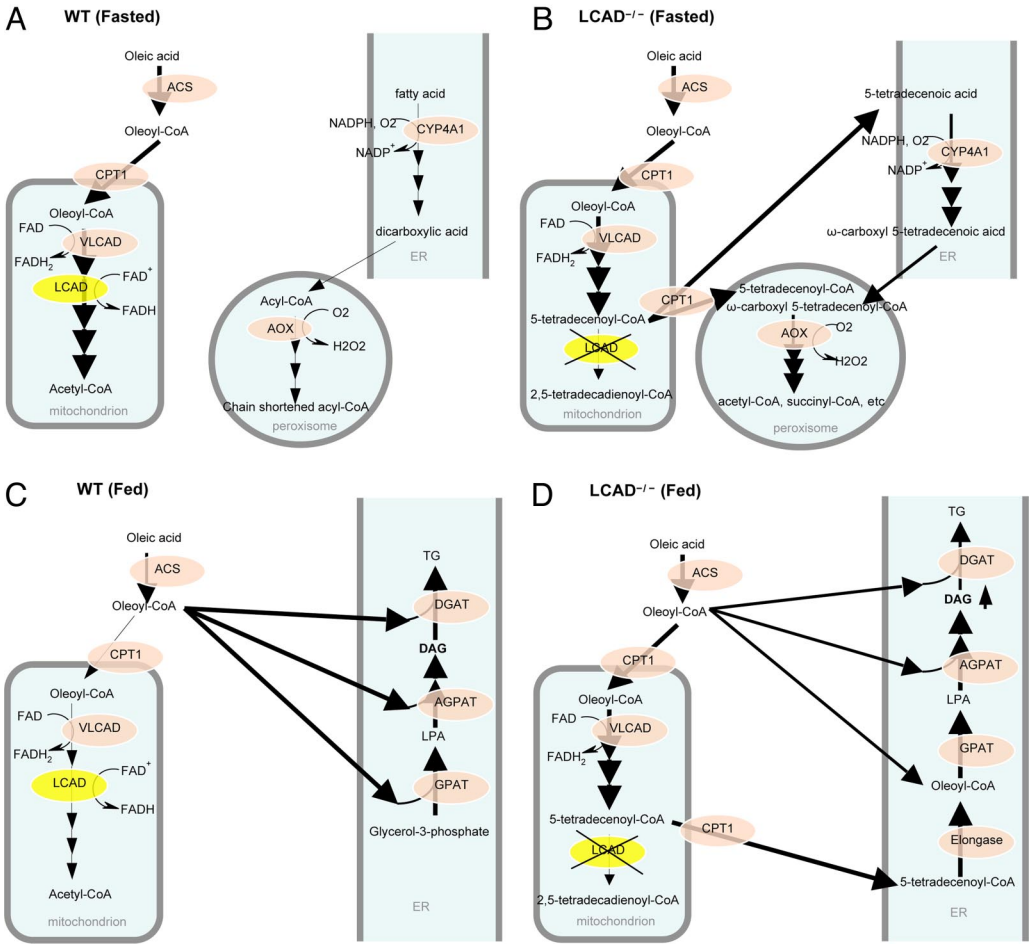

Fig. 4. Schematic diagram of oleic acid metabolism in liver of WT and *LCAD*$^{-/-}$ mice. (*A*) During fasting, WT mice have high mitochondrial oleic acid oxidation and relatively lower peroxisomal and microsomal fatty acid oxidation. (*B*) During fasting, *LCAD*$^{-/-}$ mice have reduced mitochondrial oleic acid oxidation at the level of 5-tetradecenoyl-CoA, which accumulates and is partially oxidized by peroxisomal and microsomal oxidation. (*C*) Fed WT mice convert extra oleic acid to triglyceride. (*D*) Fed *LCAD*$^{-/-}$ mice convert the accumulated 5-tetradecenoyl-CoA to diacylglycerol. ER, endoplasmic reticulum; ACS, acyl-CoA synthetase; VLCAD, very long chain acyl-CoA dehydrogenase; AOX, acyl-CoA oxidase; TG, triglyceride; DAG, diacylglyerol; LPA, lysophosphatidic acid; DGAT, diacylglycerol acyl transferase; AGPAT, acylglycerol phosphate acyl transferase; GPAT, glycerol phosphate acyl transferase.

demonstrating that ceramides do not play a major role in causing hepatic insulin resistance in this mouse model.

Diacylglycerol can be derived from either *de novo* diacylglycerol synthesis or from the breakdown of phospholipids and triglyceride. Insulin stimulates *de novo* diacylglycerol and triglyceride synthesis, whereas the regulation of triglyceride hydrolysis is controlled by insulin and catecholamines through the action of hormone-sensitive lipase (19). To examine the source of diacylglycerol accumulation in the *LCAD*$^{-/-}$ mice, we used uniformly labeled [^{13}C]oleic acid as a tracer for glycerol lipid metabolism during a hyperinsulinemic-euglycemic clamp. During fasting, oleic acid was converted to tetradecenoyl-CoA ($C_{14:1}$-CoA) and accumulated in the liver because of LCAD deficiency. Insulin stimulation resulted in the accumulation of diacylglycerol (Fig. 3*B*) and a decrease of the medium-chain acyl-CoAs (Fig. 3*C*) in liver. Our results show that the large pool of $C_{14:1}$-CoA was mostly converted to oleoyl-CoA and then to diacylglycerols after insulin stimulation, which constitutes the major part of the accumulation of diacylglycerols. In addition, from Fig. 3*B*, we can see that arachidonoyl stearoin and arachidonoyl palmitoin, the signature diacylglycerols from phospholipids hydrolysis, were not different between the two groups after insulin stimulation. This suggests that phospholipase C or D do not play a significant role in the accumulation of diacylglycerol in *LCAD*$^{-/-}$ livers after insulin stimulation. Taken together, these data suggest that the accumulation of diacylglycerols is caused by *de novo* diacylglycerol synthesis rather than phospholipid hydrolysis in this mouse model of LCAD deficiency.

Table 2. Enrichment of $^{13}C_{14}$-$C_{14:1}$ or $^{13}C_{18}$-$C_{18:1}$ groups from acyl-CoA into diacylglycerol

	$^{13}C_{14}$-$C_{14:1}$, %		$^{13}C_{18}$-$C_{18:1}$, %	
Diacylglycerol	WT	*LCAD*$^{-/-}$	WT	*LCAD*$^{-/-}$
$C_{18:1}C_{16}$	15	105*	38	43
$C_{18:1}C_{18:1}$	58	310*	27	24
$C_{18:1}C_{18:2}$	28	146*	22	26

Data represent enrichments in diacylglycerol as a percentage of enrichment in the precursor acyl-CoAs. Data represent an average of six mice per group. *, $P < 0.05$ compared with WT controls.

We also assessed whole-body metabolic parameters, using indirect calorimetry. Interestingly there was a marked difference in the diurnal pattern of fat oxidation between the WT and *LCAD*$^{-/-}$ mice (Fig. 5*A*). In the WT mice, fat oxidation varied greatly between day time and night time. During the day time, when the mice were sleeping and fasting, there was a sharp increase in fatty acid oxidation in the WT mice compared with the night time, when the mice were active and eating and during which time there was a marked suppression of fat oxidation. This marked variation in fat oxidation can most likely be attributed to activation and inhibition of mitochondrial fat oxidation by meal-induced changes in plasma insulin concentrations, which subsequently affect intracellular malonyl CoA content and carnitine palmityl transferase-1 activity. In contrast, this diurnal pattern of fat oxidation was severely blunted in the *LCAD*$^{-/-}$ mice, and the percentage of fatty acid oxidation was decrease by 27% during the day time (Fig. 5*A*). Interestingly, the *LCAD*$^{-/-}$ mice actually had a higher percentage (29%) of fatty acid oxidation compared with WT controls during the dark period when they were eating (Fig. 5*A*). It is likely that this relative increase in the percentage of fatty acid oxidation in the *LCAD*$^{-/-}$ mice

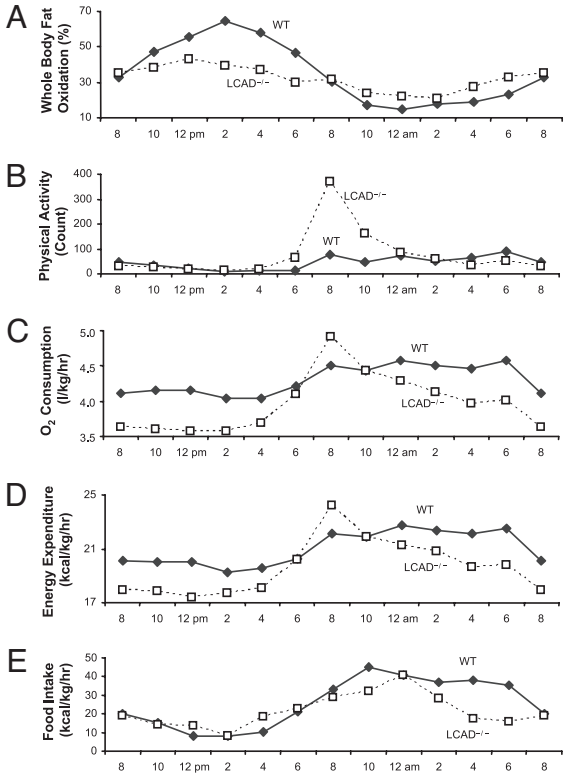

Fig. 5. Indirect calorimetry measurement during a 24-h period. (*A*) Percentage of whole-body fatty acid oxidation (derived from the measured value of respiratory quotient). (*B*) Physical activity. (*C*) Energy expenditure. (*D*) Oxygen consumption. (*E*) Food intake.

during the feeding period, when fatty acid oxidation is normally suppressed by an increase in plasma insulin concentrations, can be attributed to a compensatory increase in peroxisomal and microsomal fatty acid oxidation, which are not insulin-regulated. This hypothesis is supported by a 2- to 5-fold increase in expression of acyl-CoA oxidase and CYP4A1, which are markers of peroxisomal and microsomal content (Table 3). In contrast, no differences were found in the expression of genes involved in triglyceride synthesis, i.e., SREBP1, ChREBP, ACC1, SCD1, and DAGT2 (Table 3). Taken together, these data suggest that increased whole-body fatty content in the $LCAD^{-/-}$ mice could most likely be attributed to decreased fatty acid oxidation rather than increased lipogenesis.

Table 3. Gene expression relative to 18S in liver of WT and $LCAD^{-/-}$ mice ($\times 10^8$)

Gene	WT	$LCAD^{-/-}$
CYP4A1	175 ± 54	789 ± 283*
AOX	1,990 ± 225	3,620 ± 410*
CPT2	82 ± 6.6	107 ± 9.0*
VLCAD	58 ± 5.1	59 ± 3.6
MCAD	258 ± 21	304 ± 21
CPT1a	1,230 ± 196	990 ± 100
PPARα	155 ± 12	193 ± 22
SREBP1c	39 ± 11	36 ± 5.7
CHREBP	75 ± 15	53 ± 5.9
ACC1	13 ± 1.0	12 ± 1.4
SCD1	5,610 ± 2,260	6,290 ± 1,770
DGAT2	202 ± 20	168 ± 9.5
HSL	5.6 ± 0.74	6.3 ± 0.83
ATGL	114 ± 15	123 ± 12
PPARγ	2.0 ± 0.21	3.0 ± 0.42*
TGH	74 ± 11	130 ± 14*
SREBP2	1.8 ± 0.18	1.8 ± 0.20
LXRα	11 ± 0.9	10 ± 0.5
ACC2	6.6 ± 1.4	8.1 ± 1.1
HMGR	0.45 ± 0.04	0.64 ± 0.12

Data represent mean ± SEM of five mice per group. *, $P < 0.05$ compared with WT controls.

Our hyperinsulinemic-euglycemic clamp data show that there was surprisingly no insulin resistance in skeletal muscle of the $LCAD^{-/-}$ mice despite increases in muscle triglyceride and fatty acyl-CoA content. However, muscle diacylglycerol content was similar between the $LCAD^{-/-}$ mice and WT controls both under fasting conditions and after the hyperinsulinemic-euglycemic clamp. Taken together, these data demonstrate that fatty acyl-CoAs and triglycerides do not cause insulin resistance in skeletal muscle and that compensatory mechanisms occurred to maintain normal concentrations of diacylglycerol in skeletal muscle of the $LCAD^{-/-}$ mice. Although the compensatory mechanisms involved in the maintenance of normal intramuscular diacylglycerol concentrations in the $LCAD^{-/-}$ mice remain unknown, it does not appear to be due to up-regulation of DGAT, because, in muscle, the expression of DGAT1 and DGAT2 mRNA were not different between the two groups.

In summary, these data demonstrate that a primary defect in mitochondrial fatty acid oxidation can lead to increase in intrahepatic diacylglycerol content, which in turn activates protein kinase Cε and results in hepatic insulin resistance.

Materials and Methods

Animals. Male $LCAD^{-/-}$ and WT littermates were produced as described in ref. 11 and studied at ≈12 weeks of age. Animals were housed under controlled temperature (23°C) and lighting (12 h of light and 12 h of dark) with free access to water and standard rodent diet (Harlan Teklad, Madison, WI; catalog no. 2018S). Before experiments, all mice were fasted for 6 h, starting at 8 a.m. Body composition measurements were performed in awake mice, using a Bruker Minispec analyzer (Bruker, The Woodlands, TX). Oxygen consumption, energy expenditure, respiratory quotient, and physical activity was measured by using the Oxymax system from Columbus Instruments (Columbus, OH). All procedures were approved by the Yale University Animal Care and Use Committee.

Hyperinsulinemic-Euglycemic Clamp. At least 4 days before hyperinsulinemic-euglycemic clamp experiments, mice were anesthetized with i.p. injections of ketamine (100 mg per kg of body weight) and xylazine (10 mg per kg of body weight), and an indwelling catheter was inserted in the left internal jugular vein. The catheters were externalized through an incision in the skin flap behind the head, and the mice were returned to individual cages after the surgery. To conduct experiments in awake mice with minimal stress, a tail restraint method was used (20). A 120-min hyperinsulinemic-euglycemic clamp was conducted with a prime-continuous infusion of human insulin (Humulin; Eli Lilly, Indianapolis, IN) at a rate of 2.5 milliunits·kg^{-1}·min^{-1} (15 pmol·kg^{-1}·min^{-1}) to raise plasma insulin levels. Blood samples (20 μl) were collected at 20-min intervals for the immediate measurement of plasma glucose concentration, and 20% glucose was infused at variable rates to maintain plasma glucose at basal concentrations. Insulin-stimulated whole-body glucose flux was estimated by using a prime-continuous infusion of [3-^{3}H]glucose [10 μCi (1 Ci = 37 GBq) bolus, 0.1 μCi/min; New England Nuclear Life Science, Waltham, MA] throughout the clamps. All infusions were done by using microdialysis pumps (Microdialysis, North Chelmsford, MA). To estimate insulin-stimulated glucose uptake and metabolism in individual tissues, 2-deoxy[^{14}C]glucose (New England Nuclear Life Science) was administered as a bolus (10 μCi) at 75 min after the start of clamps. Blood samples (20 μl) were taken at 80, 85, 90, 100, 110, and 120 min after the start of clamps for the determination of plasma [^{3}H]glucose, ^3H_2O, and 2-deoxy[^{14}C]glucose concentrations. Addi-

tional blood samples were obtained before the start and at the end of clamps for measurement of plasma insulin and free fatty acid concentrations. At the end of clamps, mice were anesthetized with sodium pentobarbital overdose. Within 5 min, four muscles (soleus, gastrocnemius, tibialis anterior, and quadriceps) from both hind limbs, epididymal white adipose tissue, intrascapular brown adipose tissue, and liver were taken. Each tissue, once exposed, was dissected out within 2 s, frozen immediately by using liquid N_2-cooled aluminum blocks, and stored at −70°C for later analysis. For the fatty acid infusion experiment, [$^{13}C_{18}$]oleic acid (Spectra Stable Isotopes, Columbia, MD) in 40 mg/ml BSA was infused at a rate of 13 nmol/min for the duration of the hyperinsulinemic-euglycemic clamp, including the 2-h basal period.

Calculations. Rates of basal endogenous glucose production and insulin-stimulated whole-body glucose uptake were determined as the ratio of the [^{3}H]glucose infusion rate [disintegrations per minute (dpm)/min] to the specific activity of plasma glucose (dpm/μmol) during the final 30 min of basal and clamp periods, respectively. Endogenous glucose production during clamps was determined by subtracting the glucose infusion rate from the whole-body glucose uptake (21). Glucose uptake in individual tissues was calculated from the plasma 2-deoxy[^{14}C]glucose profile, which was fitted with a double exponential curve, using MLAB (Civilized Software, Bethesda, MD) and tissue 2-deoxyglucose-6-phosphate content as described in ref. 22. To calculate the percentage of fatty acid oxidation, we assumed that the respiratory quotient (RQ) was contributed by carbohydrate and fat oxidation only. Because carbohydrate has an RQ of 1 and fat has an RQ of 0.7, percentage of fat oxidation is derived as (1 − RQ)/0.3.

Biochemical Assays. Plasma glucose concentrations during clamps were measured by using 10 μl of plasma by a glucose oxidase method on a Glucose Analyzer II (Beckman–Coulter, Fullerton, CA), and plasma insulin concentrations were measured by radioimmunoassay, using kits from Linco Research (St. Charles, MO). Plasma fatty acid concentrations were determined by using an acyl-CoA oxidase-based colorimetric kit (Wako Chemicals, Richmond, VA). For the determination of plasma [3-^{3}H]glucose and 2-deoxy[^{14}C]glucose concentrations, plasma was deproteinized with $ZnSO_4$ and $Ba(OH)_2$, dried to remove ^3H_2O, resuspended in water, and counted in scintillation fluid (Ultima Gold; Packard, Meriden, CT) on dual channels for separation of ^{3}H and ^{14}C. The plasma concentration of ^3H_2O was determined by the difference between ^{3}H counts without and with drying. For the determination of tissue 2-deoxy[^{14}C]glucose-6-phosphate content, tissue samples were homogenized, and the supernatants were subjected to an ion-exchange column to separate 2-deoxyglucose-6-phosphate from 2-deoxyglucose, as described in ref. 20. Skeletal muscle and liver triglyceride concentrations were determined by using a triglyceride assay kit (Sigma, St. Louis, MO) and a method adapted from Storlien *et al.* (23). Long-chain acyl-CoA and diacylglycerol concentrations in skeletal muscle and liver were measured as described in ref. 24. IRS2 tyrosine phosphorylation (24), IRS1- and IRS2-associated PI3-kinase (25), Akt2 (26), and PKCε (13) assays were performed as described.

Quantitative RT-PCR-Based Gene Expression and Mitochondrial DNA Analysis. RNA was isolated from tissues, using an RNeasy kit (Qiagen, Valencia, CA) in combination with DNase I treatment. After 2 μg of total RNA was reverse transcribed (Stratagene, La Jolla, CA) with random primers, quantitative PCR was performed with a DNA Engine Opticon 2 system (MJ Research, Boston, MA), using an SYBR green quantitative polymerase chain reaction dye kit (Stratagene), and primers for different genes [see supporting information (SI) *Text*]. Product specificity was verified by running products on an agarose gel. Messenger RNA levels (ΔC_T values), normalized to 18S rRNA, were expressed by using the comparative method. 18S rRNA levels showed no statistical difference between genotypes. For mitochondrial DNA analysis, total DNA was isolated from tissues, using the DNeasy kit (Qiagen, Valentia, CA). One hundred nanograms of DNA was used for each sample for quantitative PCR, with actin as a marker for genomic DNA and ATPase 6 as a marker for mitochondrial DNA.

Statistical Analyses. Data are expressed as means ± standard error. The significance of the difference in mean values between WT and *LCAD*$^{-/-}$ mice was evaluated with the unpaired Student's *t* test.

We thank Aida Groszmann, Takamasa Higashimori, Hyo-Jeong Kim, You-Ree Cho, and Doug Hamm for their technical assistance. This study was supported by United States Public Health Service Grants R01 RR-02599 (to P.A.W.) and R01 DK-40936 and U24 DK-59635 (to G.I.S.) and an American Diabetes Association Distinguished Clinical Investigator Award (to G.I.S.)

1. Petersen KF, Befroy D, Dufour S, Dziura J, Ariyan C, Rothman DL, DiPietro L, Cline GW, Shulman GI (2003) *Science* 300:1140–1142.
2. Mootha VK, Bunkenborg J, Olsen JV, Hjerrild M, Wisniewski JR, Stahl E, Bolouri MS, Ray HN, Sihag S, Kamal M, *et al.* (2003) *Cell* 115:629–640.
3. Patti ME, Butte AJ, Crunkhorn S, Cusi K, Berria R, Kashyap S, Miyazaki Y, Kohane I, Costello M, Saccone R, *et al.* (2003) *Proc Natl Acad Sci USA* 100:8466–8471.
4. Kelly DP, Scarpulla RC (2004) *Genes Dev* 18:357–368.
5. Petersen KF, Dufour S, Befroy D, Garcia R, Shulman GI (2004) *N Engl J Med* 350:664–671.
6. Ritov VB, Menshikova EV, He J, Ferrell RE, Goodpaster BH, Kelley DE (2005) *Diabetes* 54:8–14.
7. Morino K, Petersen KF, Dufour S, Befroy D, Frattini J, Shatzkes N, Neschen S, White MF, Bilz S, Sono S, *et al.* (2005) *J Clin Invest* 115:3587–3593.
8. Petersen KF, Dufour S, Shulman GI (2005) *PLoS Med* 2:233–237.
9. Shulman GI (2000) *J Clin Invest* 106:171–176.
10. Morino K, Petersen KF, Shulman GI (2006) *Diabetes* 55(Suppl 2):S9–S15.
11. Kurtz DM, Rinaldo P, Rhead WJ, Tian L, Millington DS, Vockley J, Hamm DA, Brix AE, Lindsey JR, Pinkert CA, *et al.* (1998) *Proc Natl Acad Sci USA* 95:15592–15597.
12. Cox KB, Hamm DA, Millington DS, Matern D, Vockley J, Rinaldo P, Pinkert CA, Rhead WJ, Lindsey JR, Wood PA (2001) *Hum Mol Genet* 10:2069–2077.
13. Samuel VT, Liu ZX, Qu X, Elder BD, Bilz S, Befroy D, Romanelli AJ, Shulman GI (2004) *J Biol Chem* 279:32345–33253.
14. Banerjee RR, Rangwala SM, Shapiro JS, Rich AS, Rhoades B, Qi Y, Wang J, Rajala MW, Pocai A, Scherer PE, *et al.* (2004) *Science* 303:1195–1198.
15. Tataranni PA, Ortega EA (2005) *Diabetes* 54:917–927.
16. Kadowaki T, Yamauchi T, Kubota N, Hara K, Ueki K, Tobe K (2006) *J Clin Invest* 116:1784–1792.
17. Samuel VT, Liu ZX, Wang A, Beddow SA, Geisler JG, Kahn M, Zhang XM, Monia BP, Bhanot S, Shulman GI (2007) *J Clin Invest* 117:739–745.
18. Holland WL, Brozinick JT, Wang LP, Hawkins ED, Sargent KM, Liu Y, Narra K, Hoehn KL, Knotts TA, Siesky A, *et al.* (2007) *Cell Metab* 5:167–179.
19. Coppack SW, Jensen MD, Miles JM (1994) *J Lipid Res* 35:177–193.
20. Kim JK, Gavrilova O, Chen Y, Reitman ML, Shulman GI (2000) *J Biol Chem* 275:8456–8460.
21. Rossetti L, Giaccari A (1990) *J Clin Invest* 85:1785–1792.
22. Kim JK, Wi JK, Youn JH (1996) *Diabetes* 45:446–453.
23. Storlien LH, Jenkins AB, Chisholm DJ, Pascoe WS, Khouri S, Kraegen EW (1991) *Diabetes* 40:280–289.
24. Yu C, Chen Y, Cline GW, Zhang D, Zong H, Wang Y, Bergeron R, Kim JK, Cushman SW, Cooney GJ, *et al.* (2002) *J Biol Chem* 277:50230–50236.
25. Folli F, Saad MJ, Backer JM, Kahn CR (1992) *J Biol Chem* 267:22171–22177.
26. Alessi DR, Caudwell FB, Andjelkovic M, Hemmings BA, Cohen P (1996) *FEBS Lett* 399:333–338.